

Grouped Discrete Representation Guides Object-Centric Learning

Rongzhen Zhao, Vivienne Wang, Juho Kannala, Joni Pajarinen

{rongzhen.zhao, vi vi enne. wang, juho. kannal a, j oni . paj ari nen}@aal to. fi

Aalto University, Espoo 02150, Finland

Abstract. Similar to humans perceiving visual scenes as objects, Object-Centric Learning (OCL) can abstract dense images or videos into sparse object-level features. Transformer-based OCL handles complex textures well due to the decoding guidance of discrete representation, obtained by discretizing noisy features in image or video feature maps using template features from a codebook. However, treating features as minimal units overlooks their composing attributes, thus impeding model generalization; indexing features with natural numbers loses attribute-level commonalities and characteristics, thus diminishing heuristics for model convergence. We propose *Grouped Discrete Representation* (GDR) to address these issues by grouping features into attributes and indexing them with tuple numbers. In extensive experiments across different query initializations, dataset modalities, and model architectures, GDR consistently improves convergence and generalizability. Visualizations show that our method effectively captures attribute-level information in features. The source code will be available upon acceptance.

Keywords: object-centric learning · discrete representation · guidance · codebook · features · attributes

1 Introduction

Human vision cognition relies on the perceptual processing of visual scenes, wherein objects serve as foundational elements facilitating comprehension, reasoning, planning, and decision-making faculties [1, 2, 20]. Similarly, in artificial intelligence, object-level representation of images or videos is more versatile for visual tasks involving different modalities, compared to dense feature maps [6, 30]. Object-Centric Learning (OCL) allows representing objects and the background in visual media as sparse feature vectors, along with corresponding segmentation masks as byproducts. Noteworthily, OCL achieves this usually by plain self-supervision of reconstructing the input.

The main types of OCL include mixture-based [5, 15, 18], transformer-based [24, 26], foundation model-based [23, 32] and diffusion model-based [13, 31] ones. Transformer-based OCL, as shown in Fig. 2 left, leverages query slots to aggregate dense feature maps into sparse object-level features (vectors), and challenges slots to capture as much object information as possible through a transformer

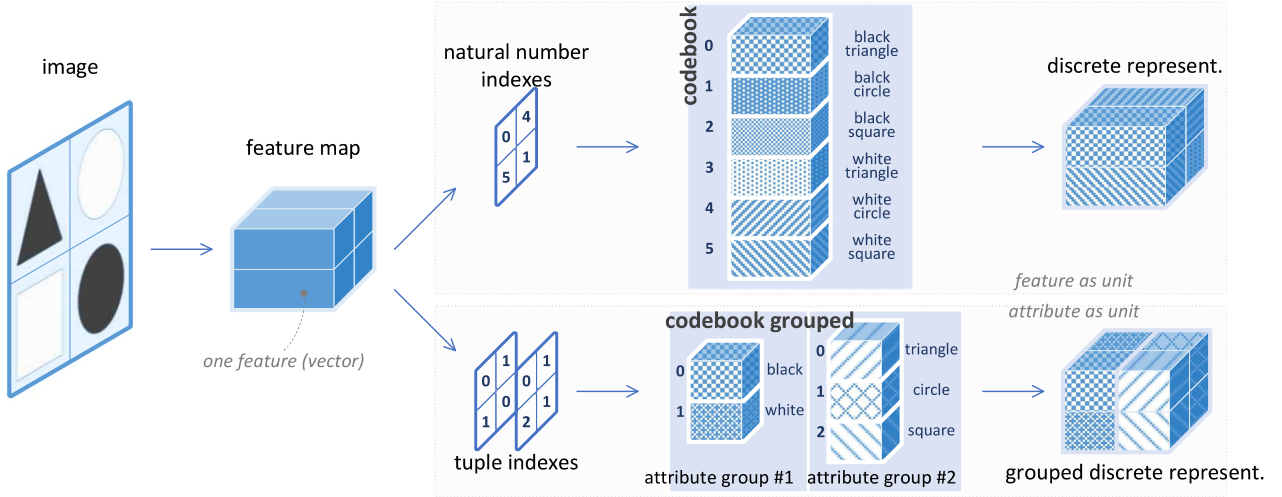


Fig. 1: Representation discretization: non-grouped vs grouped. (*upper*) Existing methods take features as units and use natural number indexes to select template features from a codebook. (*lower*) We take attributes as units and use tuple indexes to select attributes from the grouped codebook and finally combine them into features, so as to facilitate OCL convergence and generalization.

decoder to reconstruct a type of discrete representation as a classification task, rather than the input as a regression task. Guidance of the discrete representation, where noisy details in image or video feature map are eliminated, helps transformer-based OCL to process complex-textured objects in images or videos effectively. Such discrete representation is obtained firstly by a Variational Autoencoder (VAE) encoder encoding the input as continuous feature map, and then by a shared codebook replacing noisy detailed features in the continuous representation with its codes as template features. A codebook has a limited number of code vectors learned across all samples in a dataset, thereby forcing the codes to converge to more informative and generalizable representations.

However, existing transformer-based methods treat features as minimum units and entangle the attributes that compose the features, thus impeding model generalization. The natural number code indexes in these methods also fail to capture features' intrinsic information of attribute-level commonalities and characteristics, thus diminishing heuristics for model convergence.

As illustrated in Fig. 1, consider a dataset where objects (ignoring the background) consist of two attribute groups: color (black or white) and shape (triangle, square, or circle); suppose there are four objects in an image sample, for example, black-triangle, white-circle, white-square, and black-square; assume each object is downsampled into a feature vector in the feature map.

With the existing natural number indexing, six code indexes are needed to select template features from a codebook, i.e., natural numbers $0 \sim 5$ referring to black-triangle, black-circle, black-square, and so on; then the feature map can be discretized as $\begin{bmatrix} 0 & 4 \\ 5 & 1 \end{bmatrix}$. As the codes are learnt from scratch, *the indexes hold no meaning initially and provide little guiding signal for OCL*. Suppose data are evenly distributed, then *each code vector is reused with probability $\frac{1}{6}$* .

Using our method, the codebook is decomposed into two attribute groups, and features in the feature map are discretized as combinations of template attributes selected from these two groups, i.e., $[\begin{smallmatrix} 0,0 & 1,1 \\ 1,2 & 0,1 \end{smallmatrix}]$. Here identical first/second numbers in these tuples indicate that the objects have the same attribute of color/shape, and vice versa. *This provides strong learning signals for OCL, enhancing model convergence.* Moreover, each attribute group contains fewer possible values, thus *each code is reused more with probabilities $\frac{1}{2}$ and $\frac{1}{3}$, respectively, hopefully improves model generalizability.*

In short, our contributions are as follows:

- We propose *Grouped Discrete Representation* (GDR) to improve existing transformer-based OCL in both convergence and generalizability;
- We evaluate GDR’s effectiveness via extensive experiments across different dataset modalities, model architectures and query initializations;
- We provide intuitive visual interpretations of how GDR captures attribute-level commonalities and characteristics.

2 Related Work

Variational Autoencoder. Among various VAEs [8, 9, 22, 27, 28], discrete VAE (dVAE) [24] is usually employed in transformer-based OCL [13, 23, 24, 26, 29, 31, 32], thus we focus on our method’s effects on it instead of others. In typical dVAE [24, 26], the intermediate representation between the encoder and decoder is discretized with feature vectors as units and natural numbers as code indexes. We group the intermediate representation and codes into attribute-level units and perform discretization with tuples as code indexes.

Feature grouping. Grouping for better representation learning, either directly on features or on learnable parameters, [4, 7, 10, 16, 19, 33, 34] has long been explored in Convolution Neural Networks (CNN). Such a design is introduced into OCL by SysBinder [25], which groups slots directly and uses the sub-slots to aggregate object attributes from feature map to compose the final slots. We group the intermediate representation as *combinatorial* and *reusable* template attributes with a codebook, and then use the grouped discrete representation to guide the aggregation from dense feature maps into slots.

Transformer decoding. Among various OCL solutions [5, 13, 15, 18, 23, 24, 26, 31, 32], we focus on the ones based on transformer decoding, or transformer-based OCL. They utilize dVAE discrete representation to guide OCL of complex-textured objects. SLATE [24] and STEVE [26] are representatives for image and video OCL respectively. Using extra encoding as the feature map to be aggregated into slots [12, 30], rather than dVAE intermediate representation, yields SLATE⁺ and STEVE⁺. Our GDR is built upon these methods and boosts them.

Query initialization. The initial value and number of query determines the subsequent feature map aggregation into slots. As the initial scheme of shared Gaussian initialization [17, 18] was proven to be too noisy [5, 15], non-shared

random initialization [3, 12] and condition initialization. Then, schemes involving condition initialization [5, 15] (requiring extra annotation) were proposed. Some [21] argues that different samplings of the same Gaussian correspond to different instances and different Gaussians correspond to different classes. We evaluate GDR on non-shared Gaussian and condition query initialization.

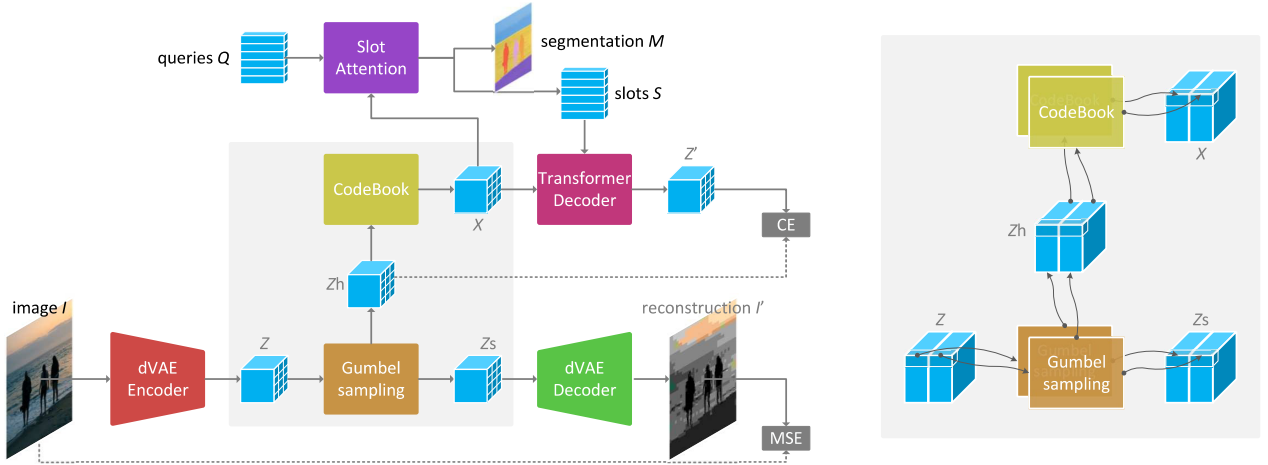


Fig. 2: Discrete representation grouping in transformer-based OCL. (*left*) Most transformer-based OCL can be simplified into this naive architecture, where the shaded area is the original representation discretization, which takes an image as input and outputs slots and object segmentation masks. (*right*) Our grouped discrete representation is obtained by grouping the intermediate feature maps along the feature/channel dimension, and then doing Gumbel sampling and codebook indexing for each group as before. All the notations here are defined in Sec. 3.1.

3 Proposed Method

We propose *Grouped Discrete Representation* (GDR), a general technique to improve transformer-based OCL [24, 26] in convergence and generalizability.

3.1 Discrete Representation

Most transformer-based OCL models can be simplified into the naive architecture of SLATE drawn in Fig. 2. Based on it, STEVE employs a stack of transformer encoder blocks as a recurrent module to convert current time step slots into next time step queries; SLATE⁺ employs an extra encoder for better feature map as input to Slot Attention; STEVE⁺ employs both the recurrent module and extra encoder. Our method is a general enhancement to them, so we take SLATE to exemplify how to change for better discrete representation.

The dVAE encoder of SLATE, essentially a CNN with small spatial down-sampling, takes an image I as input and outputs logits Z

$$Z = \text{Encoder}_{\text{dVAE}}(I) \tag{1}$$

Both soft and hard Gumbel sampling [11] are applied to Z

$$Z_s = \text{softmax}\left(\frac{Z + G}{\tau}\right) \quad (2)$$

$$Z_h = \text{argmax}\left(\frac{Z + G}{\tau}\right) \quad (3)$$

where noise $G \sim \text{Gumbel}(\mu = 0, \beta = 1)$; and τ is the temperature, typically changed from 1 to 0.1 by cosine annealing schedule during training and fixed to 0.1 during testing.

* *1st place to change. Here each feature vector in Z is sampled as a whole into a natural number index in Z_h . We propose to sample in multiple attribute groups, as formulated in Eq. (12) and Eq. (13).*

The dVAE decoder, which is a CNN with inverse up-sampling, decodes the soft sampling Z_s to reconstruct the input

$$I' = \text{Decoder}_{\text{dVAE}}(Z_s) \quad (4)$$

With the hard sampling Z_h as natural number indices, discrete representation is formed by picking template features from a codebook

$$X = \text{Codebook}(Z_h) \quad (5)$$

where Codebook is a limited-sized set of code vectors, which are randomly initialized and shared across all samples.

* *2nd place to change. Here features are taken as units, which entangles the composing attributes; and natural numbers are used as indexes, which loses features' attribute-level commonalities and characteristics. We propose to use tuple indexing and grouped codebook, as formulated in Eq. (14).*

The SlotAttention [18] aggregates the intermediate representation X into slots S with Q as query

$$S, M = \text{SlotAttention}(Q, X) \quad (6)$$

where Q is either learned Gaussian samplings or projected prior information (e.g., bounding boxes); each feature vector in slots S represents an object or background in the image; the byproduct, objects and background segmentation in the image, is obtained via argmax of attention map M along the slots dimension.

The beginning-of-sentence (BOS) token [14] is prepended to intermediate representation X for transformer-based decoding

$$X' = \mathbf{x}_{\text{BOS}} || X[: -1] \quad (7)$$

where $||$ means concatenation along feature vector dimension, and $[: -1]$ means dropping the last feature.

The modified intermediate discrete representation X' is decoded by a transformer decoder into logit Y , and read out by classifying every feature vector in Y as a natural number index in Z_h

$$Y = \text{TransformerDecoder}(X', S) \quad (8)$$

$$Z' = \text{Readout}(Y) \quad (9)$$

where TransformerDecoder is causally masked to challenge S to be informative; Readout is basically Linear plus softmax; Z' is the classification output.

The entire architecture is trained end-to-end by optimizing I' as regression (pre-training) and Z' as classification (training)

$$l_i = \mathbb{E}[\text{MSE}(I', I)] \quad (10)$$

$$l_z = \mathbb{E}[\text{CE}(Z', Z_h)] \quad (11)$$

where expectation $\mathbb{E}[\cdot]$ is performed along spatial dimensions.

3.2 Grouped Discrete Representation

Given a dataset, there are in total n possible c -dimensional discrete features that compose various objects and backgrounds. Suppose each discrete feature can be described by g attribute groups, and each attribute group has a possible attribute values, thus there are a^g possible combinations, and suppose $n = a^g$.

Then we need a codebook to represent these a^g possible discrete features, each of which is a c -dimensional template feature vector.

We propose a grouped tuple indexing scheme, as shown in Fig. 2, to realize intermediate discrete representation that preserves explicit attribute level feature.

Beforehand, let us define a grouped codebook of size $a \times g \times d$,

- There are g sub-codebooks within the codebook, and each sub-codebook is an attribute group;
- There are at most a possible attribute values in each of these attribute groups;
- Each of these attribute values is a d -dimensional sub-code vector (template attribute) and $c = g \times d$;
- Any feature can be discretized by combination of g attributes, each of which comes from one of the sub-codebooks.

Afterwards, our method needs the following two changes in the two places mentioned in Sec. 3.1.

1st, perform grouped Gumbel sampling to obtain tuple indexes for subsequent template attribute picking from the grouped codebook. Consequently, Eq. (2) and Eq. (3) are changed to:

$$Z_s = \text{softmax}\left(\frac{Z^1 + G^1}{\tau}\right) \parallel \text{softmax}\left(\frac{Z^2 + G^2}{\tau}\right) \parallel \dots \parallel \text{softmax}\left(\frac{Z^g + G^g}{\tau}\right) \quad (12)$$

$$Z_h = \operatorname{argmax}\left(\frac{Z^1 + G^1}{\tau}\right) || \operatorname{argmax}\left(\frac{Z^2 + G^2}{\tau}\right) || \dots || \operatorname{argmax}\left(\frac{Z^g + G^g}{\tau}\right) \quad (13)$$

where $Z^1 \dots Z^g$ are grouped from Z along the channel dimension; so do noises $G^1 \dots G^g$; $||$ denotes concatenation along the channel dimension.

2nd, select attributes from the sub-codebooks with every element in the tuple indexing as a corresponding index to form the intermediate discrete representation. Consequently, Eq. (5) is reformulated as:

$$X = \text{Codebook}_1(Z_h^1) || \text{Codebook}_2(Z_h^2) || \dots || \text{Codebook}_g(Z_h^g) \quad (14)$$

where $Z_h^1 \dots Z_h^g$ are grouped from Z_h along channel dimension; and aforementioned codebook are grouped into sub-codebooks $\text{Codebook}_1 \dots \text{Codebook}_g$.

Note: our hard Gumbel sampling Z_h are tuple indexes, and needs to be converted back to natural number indexes for calculating the classification loss:

$$Z_h := Z_h^1 \times a^0 + Z_h^2 \times a^1 + \dots Z_h^g \times a^{g-1} \quad (15)$$

where $Z_h^1 \dots Z_h^g$ are grouped from the original tuple Z_h along the channel dimension; and the result is the natural number Z_h .

Last, a mild loss to encourage code utilization is needed after grouping

$$l_u = -\text{entropy}(\mathbb{E}[Z_h^1]) - \text{entropy}(\mathbb{E}[Z_h^2]) - \dots \text{entropy}(\mathbb{E}[Z_h^g]) \quad (16)$$

where $\mathbb{E}[\cdot]$ is along spatial dimensions while $\text{entropy}(\cdot)$ along the channel.

3.3 Grouped vs Non-Grouped

We compare our GDR with the existing non-grouped solution as follows, whose experiment evidences are provided in the next section.

Indexing schemes. (i) Although the codebook is learnt from scratch, our grouped tuple indexing offers insightful heuristics about attribute-level similarities and differences among features in the intermediate representation, leading to better *convergence*. (ii) In contrast, the naive natural number indexing scheme in existing methods eliminates such semantic information, hindering effective heuristics for OCL model training.

Minimum units. (iii) With attribute-level decomposition, attributes are shared among all features as more reusable units. This allows for the construction of features through combinations of these attributes, potentially leading to *combinatorial generalization*. (iv) Conversely, the existing natural number indexing entangles attributes in features, which impedes the learning of generalizable attribute-level representations, especially when attributes are not uniformly distributed across datasets.

Codebook parameters. (v) Compared with the non-grouped codebook, the available number of parameters in our grouped codebook is significantly

reduced to $\frac{agd}{a^g c} = \frac{ac}{a^g c} = \frac{1}{a^{g-1}}$, e.g., only $\frac{1}{64}$ when $a = 64$, $g = 2$, $c = 256$ and $a^g = 4096$. Thus we increase c to $8c$ and use a layer normalization plus linear layer to project it back to c , resulting in $\frac{1}{1.6}$ the number of codebook parameters, still 30% less than the baselines but quite enough.

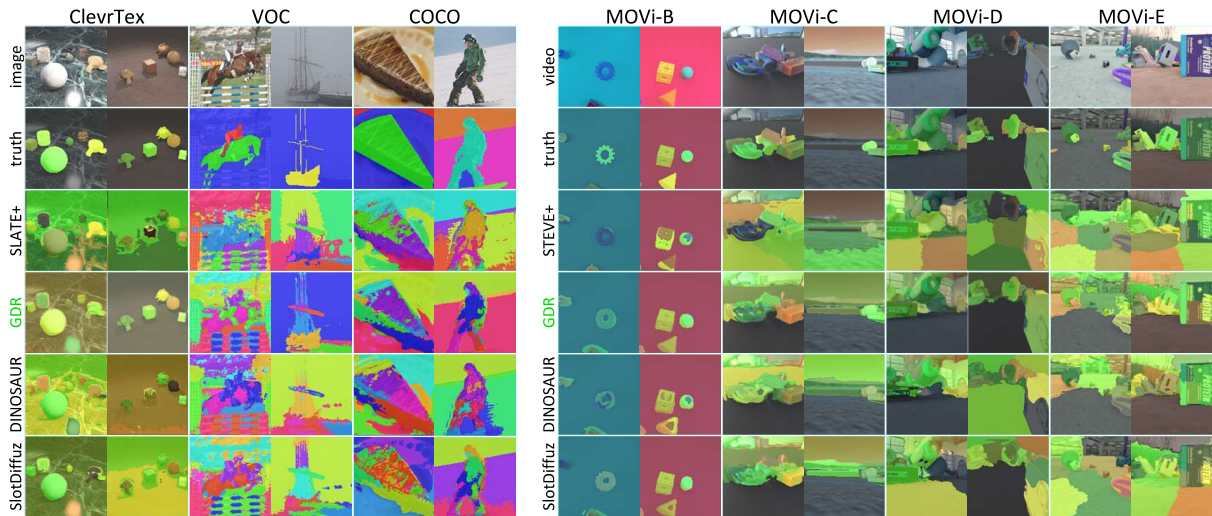


Fig. 3: Visualization of unsupervised segmentation. Left is OCL with random query on images, and right is OCL with condition query on videos. The best GDR results of settings $g2$, $g4$ and $g8$ are presented here.

4 Experiments

We conduct comprehensive experiments to address the following questions:

- Can GDR improve transformer-based OCL performance across different dataset modalities, model architectures and query initializations?
- Can GDR improve transformer-based OCL performance under zero-shot transfer among a series of datasets?
- What attribute information can GDR capture for object representation?

4.1 Experiment Overview

Models that are representatives of transformer-based OCL are included, with SLATE⁺ [24] and STEVE⁺ [26] covering *architectures* for images and videos, with SLATE [24] and SLATE⁺ [12] covering *implementations* of weak and strong baselines. Random [18] and condition [15] query *initializations* on STEVE⁺ are also covered. We include another transformer-based improver SysBinder [25], foundation-based DINOSAUR [23] and diffusion-based SlotDiffusion [31] as references, skipping the outdated SlotAttention [18] and SAVi [15]. For **fairness**, VAE encoder, decoder and codebook of all models follow that of SLATE [24]; the extra encoder follows SAVi [15]; the slot aggregation follows BO-QSA [12]; the temporal predictor follows SAVi [15]; and the other parts remain.

Datasets covering cases of single/multiple *number of objects*, cases of real-world/synthetic *sources*, and cases of image/video *modalities* are included. Birds ¹, Pets ² and Airplanes ³ are single-object real-world images; COCO ⁴ and VOC ⁵ are multi-object real-world images; ClevrTex ⁶ are multi-object synthetic images, with confusing textures; MOVi-B/C/D/E ⁷ are multi-object synthetic videos, with incremental difficulties of textures, illumination, moving views, motion blurs and so on. The data precessing follows that of SlotDiffusion [31].

Metrics that are widely used in unsupervised segmentation evaluation are adopted, including Adjusted Rand Index (ARI) ⁸, ARI of foreground (ARI_{fg}) and Intersection-over-Union of foreground (IoU) ⁹. Note: (i) ARI measures the overall segmentation accuracy, while its value is dominated by the background, which typically has the largest area; (ii) ARI_{fg} only cares foreground objects, but its high value may indicate poor background segmentation; (iii) For single object scenes, IoU is more suitable as ARI_{fg} may produce anomalous values. Thus, considering their similar definitions, we use ARI+ARI_{fg} and ARI+IoU as the overall metrics for multi- and single-object datasets, respectively.

Hyperparameters. The number of template features in the codebook is $n = a^g = 4096$. The GDR hyper-parameter g is empirically set to 2, 4 and 8, denoted as GDR@ $g2$, $g4$ and $g8$ respectively. The size of attribute groups can be determined accordingly as formulated in Sec. 3.2, i.e., (64, 64), (8, 8, 8, 8) and (2, 2, 2, 2, 4, 4, 4, 4), whose products are 4096 respectively.

4.2 Convergence

SLATE and SLATE⁺, plus improvers GDR and SysBinder, are evaluated on Birds, Pets, Airplanes, ClevrTex, VOC and COCO, with random query initialization. STEVE⁺ and our GDR variants are evaluated on MOVi-B/C/D/E, with both condition and random query initialization. DINOSAUR and SlotDiffusion are evaluated on datasets except Birds, Pets and Airplanes, with both condition and random query initialization.

Results in Fig. 3 and Fig. 4 demonstrate that our GDR mostly improves transformer-based OCL, making them even as competitive as the most advanced foundation-based and diffusion-based ones.

- As shown in Fig. 4 (a) and (b), GDR shows more effectiveness on weak model implementations, up to 30% of improvement, than on the strong.
- Comparing Fig. 4 (c) and (e), GDR contributes more improvements to image OCL than to video OCL, with random query.

¹ https://www.vision.caltech.edu/datasets/cub_200_2011

² <https://www.robots.ox.ac.uk/~vgg/data/pets>

³ <https://www.robots.ox.ac.uk/~vgg/data/bicos>

⁴ <https://cocodataset.org/#panoptic-2020>

⁵ <http://host.robots.ox.ac.uk/pascal/VOC/voc2012/index.html>

⁶ <https://www.robots.ox.ac.uk/~vgg/data/clevrtex>

⁷ <https://github.com/google-research/kubric/blob/main/challenges/movi>

⁸ https://scikit-learn.org/stable/modules/generated/sklearn.metrics.adjusted_rand_score

⁹ https://scikit-learn.org/stable/modules/generated/sklearn.metrics.jaccard_score.html

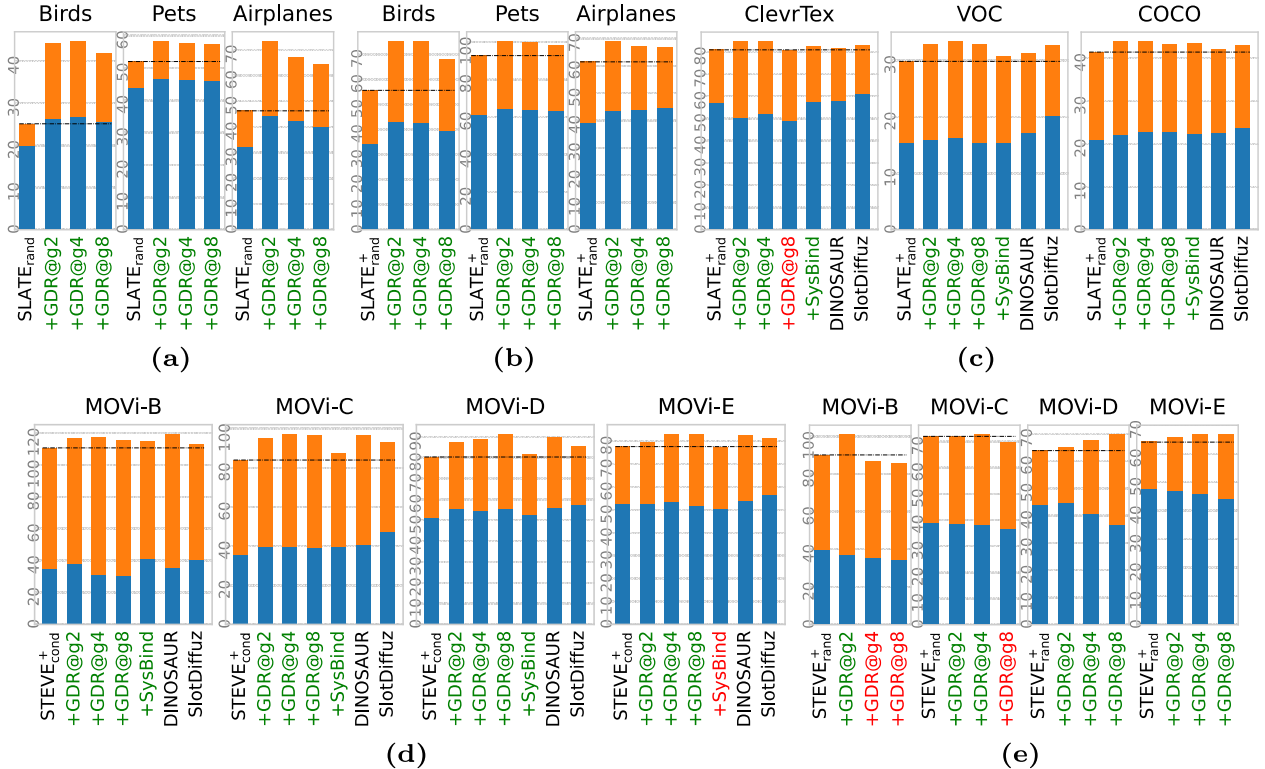


Fig. 4: Unsupervised segmentation performance measured by **ARI** (all datasets) plus **IoU** (Birds, Pets and Airplanes) or **ARI_g** (the rest) in percent. Higher is better. (seed×3)

- According to Fig. 4 (d) and (e), GDR works better with condition query than random query on video OCL.
- Compared with other methods, as shown in Fig. 4 (c), (d) and (e), our GDR improves the background more than the foreground.
- For *g* value, single-object image OCL prefers *g*2 as in Fig. 4 (a) and (b) while multi-object image OCL prefers *g*4 as in Fig. 4 (c).
- As shown in Fig. 4 (d) and (e), *g*8 can be the best choice with condition query and on videos, but not in other cases.

4.3 Generalizability

The models of STEVE⁺ with condition query mentioned in Sec. 4.2 are reused to evaluate their own zero-shot generalization among datasets MOVi-B/C/D/E. As these datasets have a varied number of objects in samples, the condition query initialization can handle this smoothly with object initial bounding boxes as query prior. And the dataset series have different scenes but with not thoroughly different objects, making them ideal for zero-shot generalization evaluation.

Results in Fig. 5 demonstrate that our GDR mostly improves transformer-based OCL in generalizability under zero-shot transfer.

- GDR of *g*2 and *g*4 always shows less performance drop when the transformer-based OCL models transfer from the source dataset to the target dataset.
- GDR of *g*8 is relatively less beneficial, and on some datasets even produces more performance drop compared with the baselines.

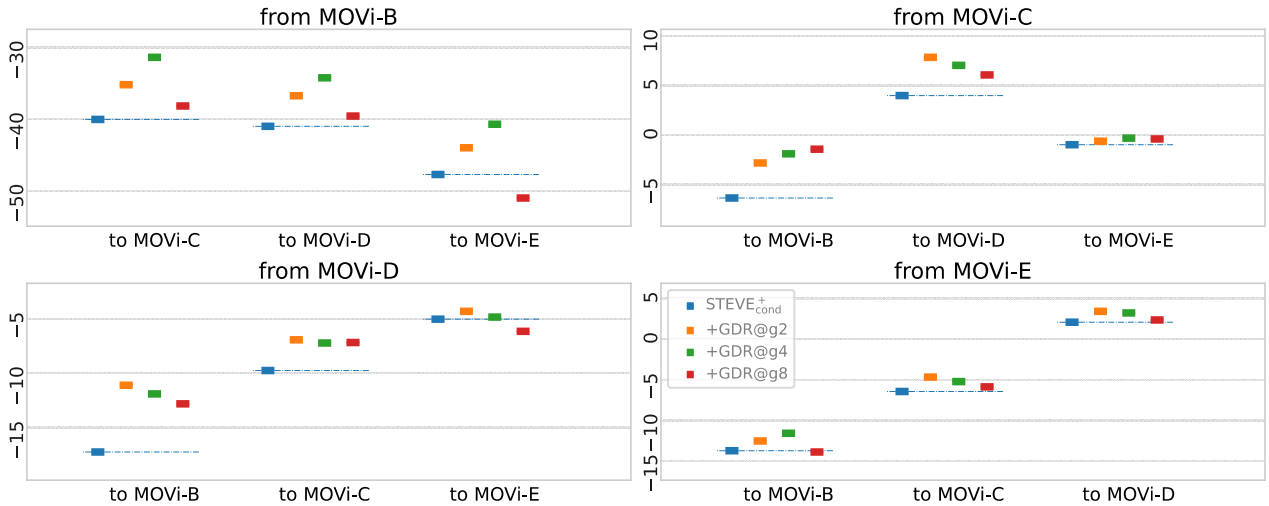


Fig. 5: Zero-shot transferred segmentation performance measured by $\Delta(\text{ARI}+\text{ARI}_{\text{fg}})$ in percent, the performance drop from source to target datasets. Higher is better. (seed $\times 3$)

4.4 Interpretability

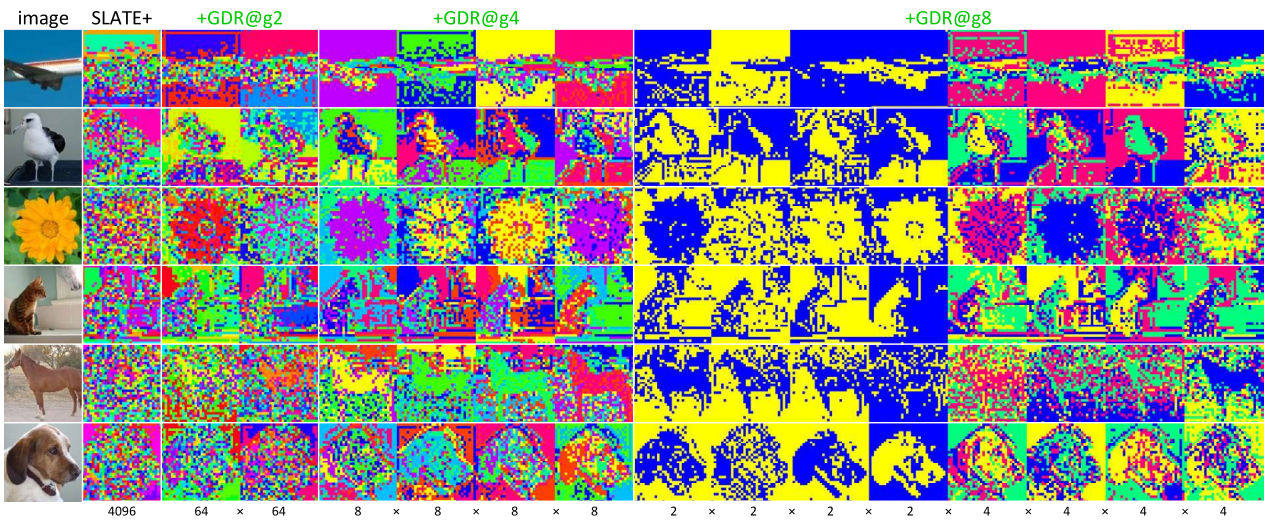


Fig. 6: Visualization of code indexes of attributes in the discrete representation. Code indexes are mapped to the HSV space. Thereby, the baselines' non-grouped indexes are visualized as single images and our GDR indexes are visualized as g images. The bottom numbers are the grouping settings, i.e., 4096 means no grouping for the baseline, (64, 64) for $g2$, (8, 8, 8, 8) for $g4$ and (2, 2, 2, 2, 4, 4, 4, 4) for $g8$, where each number limits how many possible indexes/colors are available in each column.

Codebook indexes being used to form the discrete representation allows visualizing the feature map by mapping these indexes to different colors in the HSV (Hue-Saturation-Value) color space. As for our grouped version, this can be done in similar ways and we get g HSV images. Results are shown in Fig. 6. Grouping the original features into more attribute groups, i.e., from non-grouped to $g2$ to $g4$ and $g8$, enhances the ability of the discrete representation to distinguish between different objects and the background. This suggests a stronger guidance

in optimizing OCL models. However, more intuitive discrete pattern does not guarantee better OCL performance, as discussed before. Further investigation is needed in the future.



Fig. 7: Visualization of decoded images from modified code indexes / attributes. The original image is at center, and the left and right are decoded images from the modification of the first and second attribute group of the two groups (g_2) respectively. We randomly select a segmentation area and replace the corresponding code indexes in one of the groups with a random value selected from the 64 possible code values, and decode it. Roughly, the first group learns color while the second learns texture.

Code indexes of the discrete representation can be further decoded by the dVAE decoder into an image. We can change one group of code indexes belonging to some object and decode it, to see what attributes of that object are changed. Results are shown in Fig. 7, taking g_2 as an example. The two attribute groups roughly learn attributes of color and texture—After replacing all the fist group of code indexes, the corresponding objects or background in decoded images have different colors but the same texture, while the modification for the second group loses the texture. This shows that our GDR technique truly captures attribute-level information of those intermediate discrete features.

4.5 Ablation

How the designs in GDR affect OCL performance is illustrated by ablative experiments shown in Fig. 8.

- Number of groups g in discrete representation: This is already discussed in Sec. 4.2 and Sec. 4.3. Generally, g_2 is suitable for simple datasets, g_4 is roughly the best in practice, and g_8 can score the highest but is unstable.
- Template feature dimension in the codebook: Values of $1c$, $2c$, $4c$ and $8c$ are tested, as shown in Fig. 8 (a) the lines. Clearly, larger template feature dimension yields better OCL performance, but the gain saturates near $8c$.
- Layer normalization (LN) in the codebook: As shown in Fig. 8 (a) the diamonds and crosses in the last column, LN is generally beneficial to the OCL performance, even though the performance boosts are not that significant.

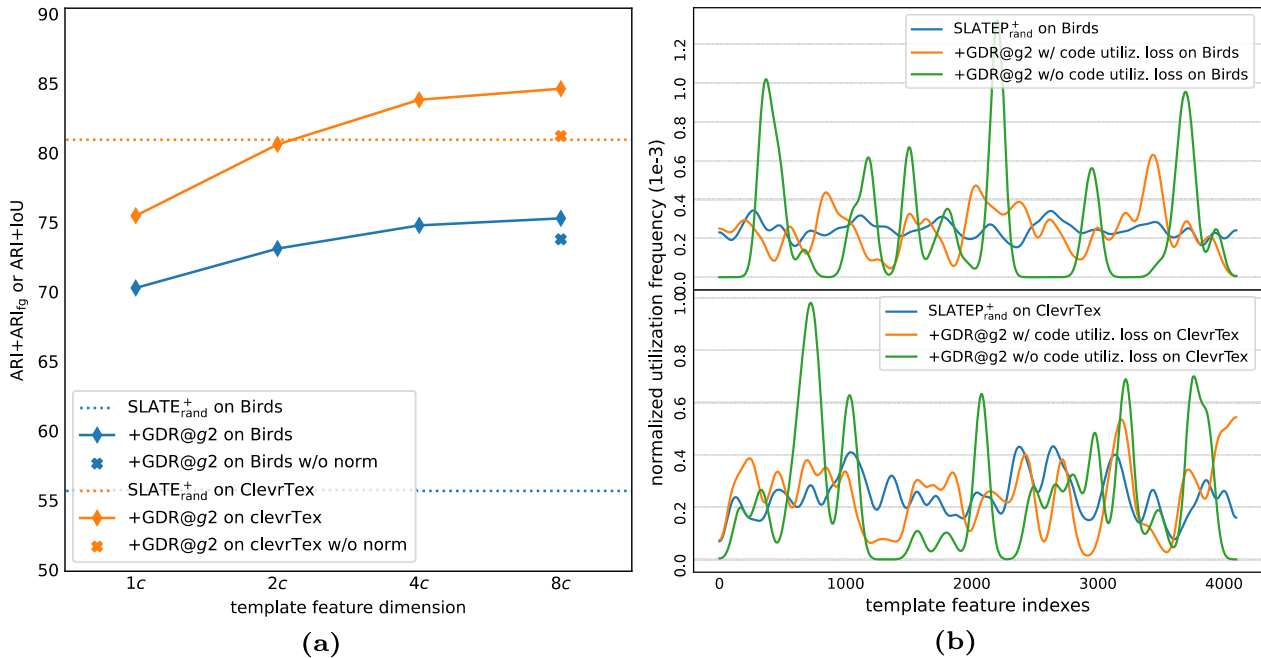


Fig. 8: Ablation studies. (a) (seed \times 5) Lines show the effects of different template feature dimensions: 1c, 2c, 4c and 8c; Crosses and diamonds in the last column show the effects of layer “norm”alization in the codebook: with vs without. (b) Curves show the effects of the code utilization loss: with vs without.

- The code utilization loss l_{u} : The code utilization is the frequency of all possible template features being used in representation discretization, as shown in Fig. 8 (b) the curves (smoothed by Gaussian kernel¹⁰ of $\sigma = 50$). Without this loss, many GDR codes are never used, while the original SLATE use all codes evenly; With it, GDR code utilization improves greatly.

5 Conclusion

We propose to decompose features into attributes by empirically grouping template feature vectors in the codebook into multiple attribute sets. This technique improves the existing transformer-based OCL methods in both convergence and generalizability. Our method also shows interesting and intuitive interpretability in terms of attribute-level discrete representation patterns. Our method mainly modifies the VAE part of current transformer-based OCL models, suggesting broader applicability to other computer vision algorithm involving a VAE module.

References

1. Bar, M.: Visual Objects in Context. Nature Reviews Neuroscience **5**(8), 617–629 (2004) **1**
2. Cavanagh, P.: Visual Cognition. Vision Research **51**(13), 1538–1551 (2011) **1**

¹⁰ https://docs.scipy.org/doc/scipy/reference/generated/scipy.ndimage.gaussian_filter1d.html

3. Chang, M., Griffiths, T., Levine, S.: Object Representations as Fixed Points: Training Iterative Refinement Algorithms with Implicit Differentiation. *NeurIPS* (2022) [4](#)
4. Chen, Y., Fan, H., Xu, B., et al.: Drop an Octave: Reducing Spatial Redundancy in Convolutional Neural Networks with Octave Convolution. *CVPR* (2019) [3](#)
5. Elsayed, G., Mahendran, A., van Steenkiste, S., Greff, K., Mozer, M.C., Kipf, T.: SAVi++: Towards End-to-End Object-Centric Learning from Real-World Videos. *NeurIPS* (2022) [1](#), [3](#), [4](#)
6. Ferraro, S., Mazzaglia, P., Verbelen, T., Dhoedt, B.: Focus: Object-Centric World Models for Robotics Manipulation. *NeurIPS IMOL* (2023) [1](#)
7. Gao, S.H., Cheng, M.M., Zhao, K., Zhang, X.Y., Yang, M.H., Torr, P.: Res2Net: A New Multi-Scale Backbone Architecture. *TPAMI* **43**(2), 652–662 (2019) [3](#)
8. Gregor, K., Papamakarios, G., Besse, F., Buesing, L., Weber, T.: Temporal Difference Variational Auto-Encoder. *ICLR* (2019) [3](#)
9. Higgins, I., Matthey, L., Pal, A., Burgess, C.P., Glorot, X., Botvinick, M.M., Mohamed, S., Lerchner, A.: beta-VAE: Learning Basic Visual Concepts With a Constrained Variational Framework. *ICLR* (2017) [3](#)
10. Huang, G., Liu, S., Van der Maaten, L., Weinberger, K.Q.: CondenseNet: An Efficient DenseNet Using Learned Group Convolutions. *CVPR* (2018) [3](#)
11. Jang, E., Gu, S., Poole, B.: Categorical Reparameterization With Gumbel-Softmax. *ICLR* (2016) [5](#)
12. Jia, B., Liu, Y., Huang, S.: Improving Object-Centric Learning With Query Optimization. *ICLR* (2023) [3](#), [4](#), [8](#)
13. Jiang, J., Deng, F., Singh, G., Ahn, S.: Object-Centric Slot Diffusion. *NeurIPS* (2023) [1](#), [3](#)
14. Jurish, B., Wurzner, K.M.: Word and Sentence Tokenization with Hidden Markov Models. *Journal for Language Technology and Computational Linguistics* **28**(2), 61–83 (2013) [5](#)
15. Kipf, T., Elsayed, G.F., Mahendran, A., Stone, A., Sabour, S., Heigold, G., Jonschkowski, R., Dosovitskiy, A., Greff, K.: Conditional Object-Centric Learning from Video. *ICLR* (2022) [1](#), [3](#), [4](#), [8](#)
16. Krizhevsky, A., Sutskever, I., Hinton, G.E.: ImageNet Classification with Deep Convolutional Neural Networks. *NeurIPS* (2012) [3](#)
17. Li, N., Eastwood, C., Fisher, R.: Learning Object-Centric Representations of Multi-Object Scenes from Multiple Views. *NeurIPS* (2020) [3](#)
18. Locatello, F., Weissenborn, D., Unterthiner, T., Mahendran, A., Heigold, G., Uszkoreit, J., Dosovitskiy, A., Kipf, T.: Object-Centric Learning with Slot Attention. *NeurIPS* (2020) [1](#), [3](#), [5](#), [8](#)
19. Ma, N., Zhang, X., Zheng, H.T., Sun, J.: ShuffleNet V2: Practical Guidelines for Efficient CNN Architecture Design. *ECCV* (2018) [3](#)
20. Palmeri, T.J., Gauthier, I.: Visual Object Understanding. *Nature Reviews Neuroscience* **5**(4), 291–303 (2004) [1](#)
21. Qian, R., Ding, S., Liu, X., Lin, D.: Semantics Meets Temporal Correspondence: Self-Supervised Object-Centric Learning in Videos. *ICCV* (2023) [4](#)
22. Razavi, A., Van den Oord, A., Vinyals, O.: Generating Diverse High-Fidelity Images With VQ-VAE-2. *NeurIPS* (2019) [3](#)
23. Seitzer, M., Horn, M., Zadaianchuk, A., et al.: Bridging the Gap To Real-World Object-Centric Learning. *ICLR* (2023) [1](#), [3](#), [8](#)
24. Singh, G., Deng, F., Ahn, S.: Illiterate DALL-E Learns to Compose. *ICLR* (2022) [1](#), [3](#), [4](#), [8](#)

25. Singh, G., Kim, Y., Ahn, S.: Neural Systematic Binder. ICLR (2023) **3, 8**
26. Singh, G., Wu, Y.F., Ahn, S.: Simple Unsupervised Object-Centric Learning for Complex and Naturalistic Videos. NeurIPS (2022) **1, 3, 4, 8**
27. Sohn, K., Lee, H., Yan, X.: Learning Structured Output Representation Using Deep Conditional Generative Models. NeurIPS (2015) **3**
28. Van Den Oord, A., Vinyals, O., et al.: Neural Discrete Representation Learning. NeurIPS (2017) **3**
29. Wang, Z., Shou, M.Z., Zhang, M.: Object-Centric Learning with Cyclic Walks Between Parts and Whole. NeurIPS (2023) **3**
30. Wu, Z., Dvornik, N., Greff, K., Kipf, T., Garg, A.: Slotformer: Unsupervised Visual Dynamics Simulation with Object-Centric Models. ICLR (2023) **1, 3**
31. Wu, Z., Hu, J., Lu, W., Gilitschenski, I., Garg, A.: SlotDiffusion: Object-Centric Generative Modeling With Diffusion Models. NeurIPS (2023) **1, 3, 8, 9**
32. Zadaianchuk, A., Seitzer, M., Martius, G.: Object-Centric Learning for Real-World Videos by Predicting Temporal Feature Similarities. NeurIPS (2023) **1, 3**
33. Zhao, R., Li, J., Wu, Z.: Convolution of Convolution: Let Kernels Spatially Collaborate. CVPR (2022) **3**
34. Zhao, R., Wu, Z., Zhang, Q.: Learnable Heterogeneous Convolution: Learning Both Topology and Strength. Neural Networks **141**, 270–280 (2021) **3**